Proceedings of the 32nd International Conference on Ocean, Offshore and Arctic Engineering OMAE 2013
June 9-14, 2013, Nantes, France

OMAE2013-10020

EMPIRICAL DEMONSTRATION OF ACAUSAL CONTROL STRATEGIES FOR WAVE ENERGY CONVERTERS

James Eder
Ocean Power Technologies
Pennington, NJ, USA

James Bretl
Ocean Power Technologies
Pennington, NJ, USA

Kathleen Edwards
Ocean Power Technologies
Pennington, NJ, USA

ABSTRACT

The benefit of acausal control strategies for Wave Energy Convertors (WECs) is empirically demonstrated in a wave tank. An upstream wave gage is used to provide real time predictions of the wave elevation at the WEC's location. Using a sub-optimal control strategy based upon complex conjugate control, these predictions are used to generate real time force commands for the Power Take Off (PTO) system. Empirical comparisons are made between the acausal control strategy and a simple linear damping approach.

I. INTRODUCTION

Significant reductions in the overall cost per unit energy are required to support rapid large scale commercialization of Wave Energy Converters (WEC). Perhaps the most promising opportunity for reducing the WEC cost of energy lies in the development of acausal control strategies.

At the present state of technical development, there exists a wide gap between the amount of energy which is theoretically available for a given WEC shape and that which is actually extracted by the device during operation.

It is known in the industry that acausal control schemes [1] such as complex conjugate control [2] provide one path toward closing this gap between theory and practice. However, there are some significant obstacles which prevent its realization, including acausality, reactive power flow, the presence of Power Take Off (PTO) limits as well as the presence of non-linearities in the physical system.

Acausality refers to the fact that the optimal control scheme requires a prediction of future wave elevation or excitation force. It is also known that the optimal control strategy requires high levels of bi-directional power flow, the peaks and troughs of which can be more than five times the device rating. Optimal control also results in peak forces, velocities, displacements and power values which drive significant costs into the machinery. And finally, optimal control schemes are typically based upon linear hydrodynamic theory. Therefore, they do not take into account significant non-linearities such as drag, variations in the wetted surface, bumper impacts and friction.

Each of these effects will reduce the maximum upper bound of power that can be extracted. Further, there exists no analytic, closed form control scheme which will produce optimal power under these real world challenges. The challenge, therefore, is to develop a suitable, sub-optimal, strategy which addresses these issues while maintaining an advantage over the simpler approaches, such as linear damping.

Although each of these issues has been theoretically investigated in some detail over past few years, limited experimental data is available which physically demonstrates the benefit of such control schemes. To this end, this paper presents empirical results for a model scale WEC using an acausal control strategy based upon complex conjugate control, but adapted to accommodate these practical challenges.

II. THEORY

The focus here is WECs that move vertically (heave) in response to waves in order to generate power. Assuming a harmonic dependence of all variables, the linear governing equation [2] is given as

$$Z_i(\omega)v(\omega) - F_{PTO}(\omega) = F_e(\omega). \quad (1)$$

The intrinsic impedance of the WEC, $Z_i(\omega)$, in Eq. (1) is given by

$$Z_i(\omega) = i\omega[m + m_a(\omega)] + R(\omega) + \frac{1}{i\omega}S_f \quad (2)$$

The term on the right hand side of Eq. (1) is the excitation force, $F_e(\omega)$ which represents the force provided by the wave on the WEC. It is given by the following equation.

$$F_e(\omega) = f_i(\omega)\eta(\omega) \quad (3)$$

The other terms in Eq. (1) and (2) are defined as follows:

ω	Angular frequency
$v(\omega)$	Heave velocity of PTO
$F_{PTO}(\omega)$	PTO force
$f_i(\omega)$	Excitation force transfer function
$\eta(\omega)$	Undisturbed wave elevation at the WEC
m	Mass of WEC
$m_a(\omega)$	Added mass
$R(\omega)$	Radiation damping
S_f	Hydrostatic stiffness

In a feedback control law, the PTO force can be determined by the following equation.

$$F_{PTO}(\omega) = Z_{PTO}(\omega)v(\omega) \quad (4)$$

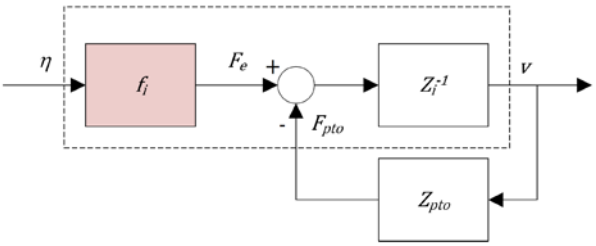

Fig. 1. Block diagram of a WEC operating in heave

The PTO impedance term, $Z_{PTO}(\omega)$ can be viewed as the transfer function which relates the PTO force as a function of the measured heave velocity. One of the common, basic WEC control strategies is for the PTO impedance to be equal to a constant value, i.e. $Z_{PTO}(\omega) = \beta$. In this case, the PTO acts as a simple linear damper with a PTO force proportional to the instantaneous WEC velocity.

Equations (1)-(4) fully describe a dynamic system. While these equations are expressed in the frequency domain, they can equivalently also be expressed in the time domain and represented by a block diagram as in Fig. 1. In this and all block diagrams that follow, shaded boxes represent transfer functions which are not purely causal. In this example, the excitation transfer force function is non-causal. The non-causal nature of this transfer function is due in part to the finite size of the WEC geometry as well as the dispersive nature of wave propagation.

The dashed box surrounding the upper line of transfer functions in Fig. 1 represents the physical world which cannot be altered by the controller. Transfer functions outside of the box represent controller transfer functions which can be engineered to maximize the power absorbed by the WEC.
The product of F_{PTO} and v provide the instantaneous power absorbed by the WEC as a function of time. In the general case, this power will be both positive and negative. According to this sign convention, positive power is absorbed by the WEC, while negative power corresponds to instances where power is sent out into the sea via the waves generated by the WEC's motion. The goal is to maximize the *average* power absorbed by the WEC over a period long enough to remove wave-to-wave variability. It has been established [2] that the maximum possible average power is extracted when the PTO impedance is given by the following expression.

$$Z_{PTO}(\omega) = Z_i^*(\omega) \quad (5)$$

The superscript (*) represents the complex conjugate operation and this control strategy is known as complex conjugate control. Under this control scheme, the average power extracted at each frequency is given by the following equation.

$$\langle \overline{P}(\omega) \rangle = \frac{|f_i(\omega)|^2}{8R(\omega)}|\eta(\omega)|^2 \quad (6)$$

In the previous equation, the brackets $\langle\ \rangle$ represent the time averaged power over a single period of the frequency in question, while the overbar, $\overline{P}$ represents the fact that the resulting power, $\langle \overline{P}(\omega) \rangle$ is maximized when complex conjugate control is applied.

There are two features of this control strategy that distinguish it from more basic control strategies. First, unlike linear damping control where the power flow is uni-directional, complex conjugate control requires bi-directional, or reactive, power flow. This has dramatic ramifications when considering PTOs with less than perfect efficiencies in the conversion of mechanical to electrical power, as it is desired to maximize the converted electrical power rather than the absorbed mechanical power. This issue will be addressed in a later section. Second, the optimal PTO transfer function, here $Z_i^*(\omega)$, that relates the PTO force to the WEC velocity is anti-causal. Therefore, complex conjugate control as given by Eq. (5) and shown in Fig. 1 is not directly realizable by a real time controller.

A. Sub-Optimal Control using an Upstream Wave Sensor

In order to resolve the causality issue just discussed, it has been proposed [2] that upstream sensors can be used to

provide necessary prediction of the future wave elevation (and excitation force) at the WEC's location. The required length of this prediction is determined by hydrodynamic coefficients of the WEC in question and typically ranges from 20-50 s [3] for a full size device. Therefore, the problem is to define a new transfer function which relates the PTO force to the measurement of the upstream wave sensor.

Consider a WEC and a single upstream wave elevation sensor located a distance d from the center of the WEC. The sensor provides the controller with a real time measurement of the wave elevation η_s at the sensor location.

At present, only long crested waves coming from a single direction are considered. Later, this approach can be extended to the more general case of short crested, multi-directional seas, in which the single wave sensor for this case is replaced by an array of sensors positioned so as to provide a suitable prediction of the incident wave field from one or more dominate directions for a particular site. [4], [5]

It can be shown that for a system operating under complex conjugate control that the block diagram shown in Fig. 1 can be rearranged as shown in Fig. 2.

Here the transfer function $\Gamma'(\omega)$ that provides the relationship between the upstream wave sensor η_s and the PTO Force F_{PTO} is given by the following expression.

$$\Gamma'(\omega) = \frac{F_{PTO}(\omega)}{\eta_S(\omega)} = e^{[-ik(\omega)d]} \frac{f_i(\omega) Z_i^*(\omega)}{2R(\omega)} \quad (7)$$

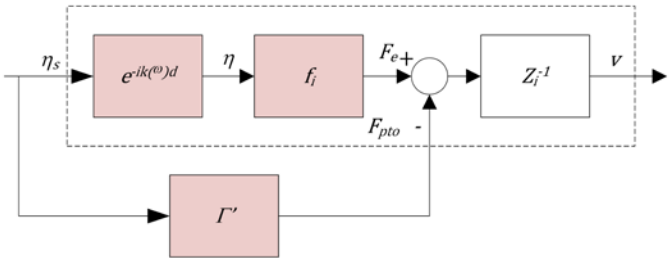

Fig. 2. Block diagram of a WEC operation under complex conjugate control using an upstream wave sensor to provide a prediction.

The exponential term, $e^{[-ik(\omega)d]}$, accounts for the propagation delay of the wave as it propagates from the upstream sensor towards the WEC.

For gravity waves propagating in water of a depth h the wavenumber $k(\omega)$ satisfies the dispersion equation.

$$\omega^2 = gk(\omega)\tanh[k(\omega)h] \quad (8)$$

Strictly speaking, the $\Gamma'(\omega)$ transfer function shown in Fig. 2 remains non-causal even though an upstream sensor has been added. This non-causality is due in part to the fact that higher wave velocities for the low frequency portion of the spectrum may yield insufficient prediction times. Fortunately, there is typically little available energy in the wave field where these conditions apply allowing a sub-optimal, yet causal approximation to made. For a real time digital controller, this transfer function may be implemented in the form of a digital filter.

B. Handling PTO Limits and Inefficiencies

The preceding development ignores the effect of PTO limits and their inefficiencies. PTO limits may take the form of finite stroke, force, power limits. Further, inefficiencies in the PTO can result in dramatic power losses for cases involving a large amount of reactive power. Approaches such as Model Predictive Control (MPC) [6], [7] have shown some promise in performing the constrained optimization problem. With this method, optimum force or velocity profiles are generated within the prediction horizon which attempt to maximize the produced electrical power, while simultaneously satisfying the PTO constraints. The nonlinearities imposed by the PTO constraints can be thought of as thresholds that are applied to the optimal solution for the PTO force and its instantaneous trajectory.

Ocean Power Technologies has developed a similar algorithm to MPC which addresses these limits, while attempting to maximize the output electrical power. The term "attempting" is used here since there exists no closed form solution which can guarantee that the true maximum has been obtained. The proprietary algorithm embeds several adjustable parameters. These parameters allow for errors in the hydrodynamic model and weight the relative importance of respecting the various limits within the system. With aid of a wave tank test, acceptable settings can be determined and fixed as part of the final system.

III. Experimental Setup

A wave tank test was conducted to compare the average power resulting from the acausal control strategy just described to the power resulting from a linear damping control law. For proprietary reasons, the exact scale and corresponding full scale dimensions of the WEC are intentionally not provided in this paper. All results and power values are consistently provided in model scale to establish comparisons between control schemes.

The point absorber model shown in Fig. 3 was equipped with an active PTO capable of reactive power. The PTO was installed inside a cylindrical spar. A nominally toroid-shaped float was positioned around the spar and guided by a set of external rails which act as a linear bearing for the relative motion between the float and spar.

The model was controlled by a digital controller with a servo update rate of 50 Hz. The controller was responsible for both control and data acquisition functions. A human machine interface program was provided on a desktop PC to aid in setting parameters and initiating the tests. Both the controller and desktop PC were located outside the tank and were tethered to the model by three separate cables.

The PTO had a maximum allowed linear force limit, although other lower force limits could be programmed into the system so as to determine the effect of PTO force capability on power capture. The PTO stroke was limited.

Mechanical power was measured as the product of PTO force and velocity. To measure the actual PTO force, a load cell was installed between the system's linear motor and a thrust rod connected to the toriod-shaped float. A high resolution linear encoder was used to measure the relative position of the float and the spar. The PTO velocity was obtained by numerically differentiating the position signal. For each run, the average mechanical power over the test duration was calculated.

Since the model's PTO efficiency is not indicative of a full scale device, it is not desirable to directly measure the electrical power generated by the model. Rather, an efficiency model is used to estimate the net electrical power based upon the measured mechanical input profiles of force and velocity. The parameters of this efficiency model would, in the ideal case, be based upon physical measurement taken from full scale bench tests of the PTO system. Once these parameters are measured, they can be programmed into the control law so that net electrical power, rather than mechanical power, can be optimized by the system.

A wave gage was positioned between the WEC's location and the wave-board. The gage was located at an "upstream" position. An analog signal proportional to the instantaneous wave elevation is provided as input to the real time controller for the model.

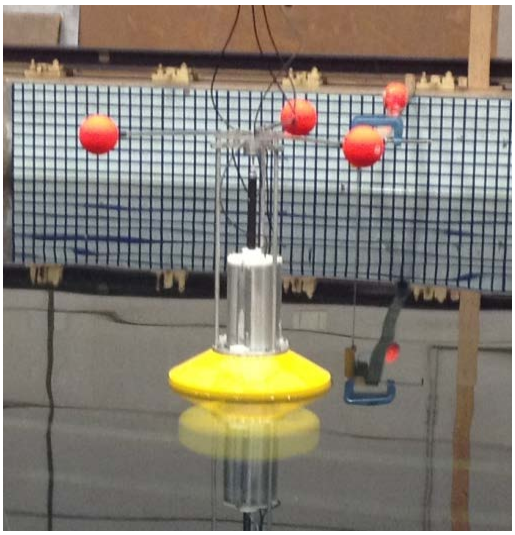

Fig. 3. Test model used in this study

Seven irregular sea states were selected for testing. These sea states were all long crested seas with a Bretschneider spectrum with the following significant wave height and average periods [H_s (mm),T_a (s)] values: [50, 1.12], [50, 1.57], [50, 2.01], [100, 1.57], [100, 2.01], [150, 2.01] and [150, 2.24].

The capacity factor for WECs stands to gain most from improved performance in lower sea states. Performance of the control becomes less important as the sea state tends toward the higher non-linear conditions. Therefore, sea states were chosen to represent a range of the most commonly occurring scaled sea conditions but with a slight focus on lower sea states. A single six minute realization of each sea state was repeated throughout the test program so as to isolate on the effect of various control strategies.

IV. Results

A. Linear Damping Control Strategy

Each sea state was tested with linear damping control to establish a baseline. In order for a valid comparison to be made, the optimal damping value was first determined for the H_s=100 mm, T_a=1.57 s sea state. The results of this optimization is shown in Fig. 4, where an optimum power is achieved with a moderate damping value. The resulting experimental curve is quite smooth, thus indicating that the experimental measurements are relatively noise free. Next, this optimized damping value was used for all other sea states. Table I shows the average mechanical power extracted by the PTO.

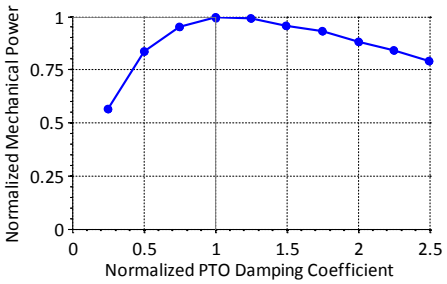

Fig. 4. Average power for Hs=100 mm, Ta=1.57 s versus linear damping setting. Values normalized by their value at peak power.

TABLE I: SUMMARY OF MECHANICAL POWER OUTPUT AT VARIOUS SEA STATES FOR LINEAR DAMPING CONTROL.

H_s (mm) \ T_a (s)	0.67	0.89	1.12	1.34	1.57	1.79	2.01	2.24	2.46	2.68
200										
175										
150							**1.25**	**1.13**		
125										
100					**0.63**		**0.58**			
75										
50			**0.12**		**0.17**		**0.14**			
25										

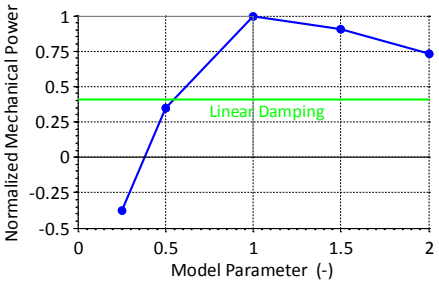

Fig. 5: Optimization of a single control parameter at Hs=50 mm, Ta=1.57 s using acausal control. The average mechanical power for linear damping control in this sea state is shown for comparison as the bold horizontal line. Values are normalized by their value at peak power.

B. Acausal Control Strategy

Similar to the linear damping case, the various parameters which alter the performance of the algorithm were first optimized on selected sea states before a full set of tests were completed across all sea states. The result of one such optimization at H_s=50 mm, T_a=1.57 s is shown in Fig. 5. The figure also shows a horizontal line indicating the power that was extracted for this sea state using linear damping control.

The altered model parameter on the x axis adjusts the mathematical model within the controller. The setting has been normalized so that the optimum value for this setting is unity. As well, power is normalized by its optimum value. It should be apparent that low or even negative power can result if the controller's model of the WEC's dynamics disagrees significantly with the actual behavior of the WEC. Here, it can be seen that for parameter settings less than 0.6, the resulting power is less than that which was obtained using linear damping control, and negative power results is the setting is less than about 0.4. This is one of the crucial ramifications of a strategy that includes reactive power flow. It can also be seen that the optimum setting results in a power level which approximately 2.6 times greater than the optimized power that was obtained for the linear damping case.

Once all the various model settings were optimized in a similar manner, a single set of fixed control parameters was used across all seven sea states. The results of this are shown in Table II.

TABLE II: SUMMARY OF MECHANICAL POWER OUTPUT AT VARIOUS SEA STATES FOR ACAUSAL CONTROL.

H_s (mm) \ T_a (s)	0.67	0.89	1.12	1.34	1.57	1.79	2.01	2.24	2.46	2.68
175										
150							**2.15**	**1.86**		
125										
100					**1.43**		**1.3**			
75										
50			**0.26**		**0.53**		**0.44**			
25										

TABLE III. RATIO OF MECHANICAL POWER RESULTING FROM ACAUSAL CONTROL TO LINEAR DAMPING CONTROL ACROSS VARIOUS SEA STATES

H_s (mm) \ T_a (s)	0.67	0.89	1.12	1.34	1.57	1.79	2.01	2.24	2.46	2.68
200										
175										
150							**1.7**	**1.6**		
125										
100					**2.3**		**2.2**			
75										
50			**2.2**		**3.2**		**3.1**			
25										

The benefit of acausal control over linear damping can be analyzed by taking the ratio of the two alternatives for each sea state. Table III summarizes these results. It can be seen that acausal control results in mechanical power improvements of 1.6 to 3.2 times that for linear damping control. In general, the results show a greater improvement at lower sea states compared with higher sea states.

This should not be surprising since lower sea conditions are more likely to follow the linear behavior upon with the control strategy is based. One significant observation for the acausal control in higher sea states was that the float motions were quite large. This caused large variations in the instantaneous wetted surface area; so much that the entire float would become submerged, followed by a full breach of the float. Therefore, it is envisioned that some modifications to the float geometry should be considered so as to better leverage the benefit of acausal control where greater WEC motions are in effect.

C. Inefficient PTO

The preceding results demonstrate a benefit of acausal control over linear damping control considering the absorbed mechanical power. It is paramount however that such an algorithm can also yield a significant benefit over conventional control schemes regarding the generated electrical power. Real PTOs have less than 100% efficiency. Therefore, large reactive power flows which net a relatively small, yet optimal, mechanical power could easily result in small or no improvement over basic control algorithms when PTO efficiencies are considered.

To account for this possibility, the acausal control algorithm included a means to limit the amount of reactive power that is applied at any point in the test. Several runs were made at a given sea state in which the maximum allowed instantaneous power was adjusted.

The results of this test are shown in Fig. 6a-c. The sea states tested here are a. (H_s=50 mm, T_a=1.57 s), b. (H_s=100 mm, T_a=1.57) and c. (H_s=150, T_a=2.01 s). As expected, the results do show some reduction in the absorbed mechanical power as reactive power is varied. However, even when the measured maximum reactive component of the mechanical power was

near zero, a significant benefit of acausal control over linear damping still remained.

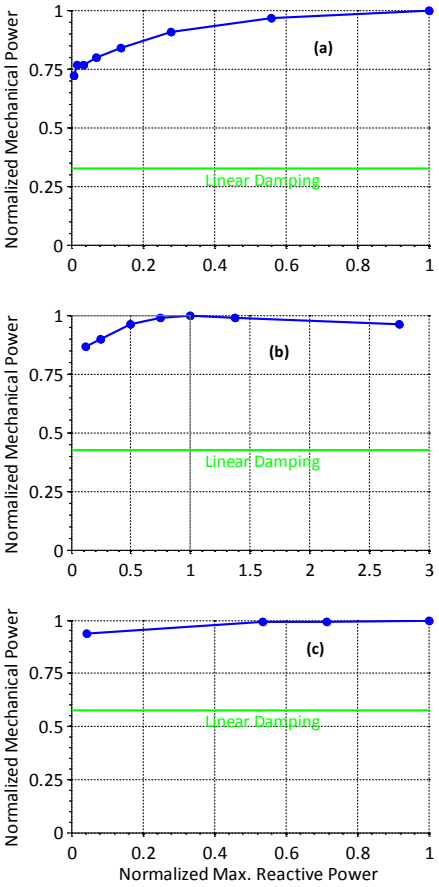

Fig. 6. Absorbed mechanical power as a function of reactive power across various sea states. Values normalized by their value at max power. Figures (a), (b) and (c) represent (H_s, T_a) sea states of (50 mm, 1.57s), (100 mm, 1.57 s), and (150 mm, 2.01 s)

Comparing the ratio of the acausal control power to the linear damping power for the lowest maximum reactive power shows improvements of 2.5, 2.0 and 1.7 were respectively measured for Hs, T_a sea states of (50 mm, 1.57s), (100 mm, 1.57 s), and (150 mm, 2.01 s). It can therefore be expected that these improvements represent lower bounds for the electrical power realized using acausal controls, since the inefficiencies of the PTO would likely be equal for linear damping.

D. Force Limits

One of the biggest challenges in the commercialization of WECs is the large ratio of peak to average ratings for the various components. A key driver in the cost of a WEC device is the maximum PTO force capability of the motor. It is therefore important to make an assessment on the incremental benefit of greater PTO force capability. Given the nature of the greater precision in the commanded force that is required by acausal control, it is important to understand the power reduction which occurs as more restrictive limits on the maximum PTO force are enforced [8]. This is particularly true for higher sea states, where finite strokes also further constrain the problem.

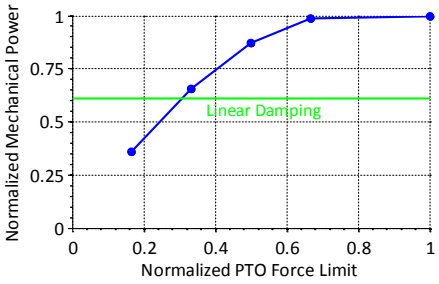

Fig. 7. Average mech. power versus force limit for H_s=150 mm, T_a=2.01 s. Values normalized by their value at max power.

To study this effect, a method was included in the acausal control algorithm to limit the maximum force that would be applied by the PTO. Various force limits were applied at a sea state corresponding to Hs=150 mm, Ta=2.01 s. The results of this test are shown in Fig. 7. It should be noted that original commanded PTO force for this state would have a maximum value which exceeds the PTO limit. However, the occurrence of instances where this maximum was exceeded was quite low. Even so, the results indicate insignificant reduction in the absorbed mechanical power as long as the PTO force exceeds a moderate value. This highlights a significant opportunity to reduce the capital cost of a WEC, while still maintaining an advantage of 1.6X over linear damping control. The results also show that it is not essential for the actual PTO force profile to precisely agree with the optimal profile which complex conjugate control would prescribe.

E. Estimate of Average Annual Benefit of Acausal Control

The power results shown in Tables I and II represent the average mechanical power from the tested sea states. In order make an assessment on the possible benefit of an acausal control, these empirical results have to be extrapolated to estimate the resulting electrical power and extended across a greater range of sea states.

The process of estimating the electrical power from the mechanical power is described first. For each sea state tested, the instantaneous mechanical power profile is calculated as the product of PTO force as measured by the load cell and the velocity as measured by the encoder. Since the control used to generate the data in Table II had no limits placed on the reactive power, the power flow is bi-directional. An example of one such profile is given in Fig. 8.

A simple constant efficiency model is used to estimate the electrical profile. Under this scheme, the electrical power profile $p_{elec}(t)$, is given by the following equation.

$$p_{elec}(t) = \begin{cases} \frac{p_{mech}(t)}{\eta_{PTO}}, & p_{mech}(t) < 0 \\ \eta_{PTO} p_{mech}(t), & p_{mech}(t) \geq 0 \end{cases} \quad (9)$$

In the previous equation, $p_{mech}(t)$ is the mechanical power profile and η_{PTO} represents the PTO efficiency. It can be seen

that this approach accounts for the fact that power is lost during both generating and motoring instances.

The proposed model is not rigorous; the true PTO efficiency is more complicated function of the exact force and velocity profile followed by the PTO, not just their product as is proposed. The development of this precise efficiency map will be the subject of future investigations.

In the present case, a constant efficiency is used for both generating and motoring instances. The chosen value is representative of the losses which exist between the linear mechanical power and the DC bus of the inverter which connects to the permanent magnet generator/motor. All other conversion and transmission losses between the DC bus and grid connection are considered equal between the two control schemes and therefore are not considered here. Figure 9 shows the result of this calculation based upon the mechanical profile shown in Fig. 8.

The average electrical power was then calculated for each profile to provide an estimate for the electrical power at each tested sea state. The results were tabulated into power matrices with entries at all tested sea states. However, the tested sea states only represented a portion of all sea states composing the power matrix, but a full power matrix is required to estimate the annual averaged power production at a site.

In order to fill in the missing sea states, an objective mapping scheme [9] was used to blend the measured values into empty regions of the table, given a chosen range of influence of each test point and an acceptable error in the resulting map. Since the tested sea states were chosen to capture the expected shape of the power vs. sea state surface, the map should be a reasonable representation of the actual power matrix. It was necessary to set power values at H_s=25 mm to a quarter of their values at H_s=50 mm since the mapped decay was too sharp. Tables IV and V provide these extrapolated results for both the linear damping and acausal control cases respectively. The measured sea states are in bold to distinguish them from the extrapolated values.

Once this is done, the average annual power from both control schemes can be obtained if one considers the Joint Probability Distribution (JPD) for the proposed deployment site. The JPD expresses the probability of occurrence for each sea state. The sum of the values in the JPD is identically equal to one. Table VI provides a scaled version of a JPD for a notional deployment site.

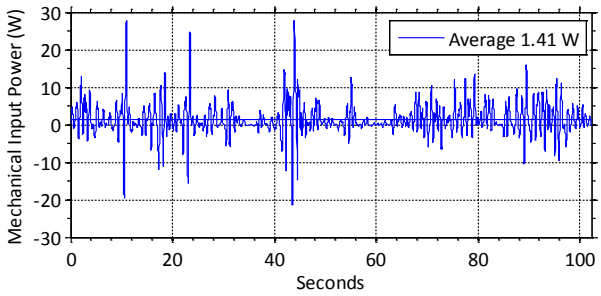

Fig. 8. Mechanical power profile obtained using acausal control for H_s=100 mm, Ta=1.57 s. Positive power indicates generation and negative power represents motoring. The average power is shown as a dashed line.

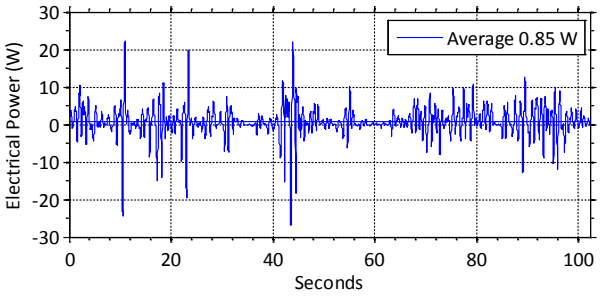

Fig. 9. Estimated electrical power profile obtained using acausal control for H_s=100 mm, Ta=1.57 s. Positive power indicates generation and negative power represents motoring. The average power is shown as a dashed line.

Multiplying the average electrical power at each sea state (Tables IV and V) by the probability of occurrence for that sea state (Table VI) and summing the result for all sea states provides the average annual power for the WEC. These calculations reveal respective average annual electrical powers of 0.50 W and 0.30 W for acausal and linear damping control schemes.

TABLE IV. ELECTRICAL POWER MATRIX FOR THE LINEAR DAMPING CONTROL CASE. RED (BOLD) VALUES CORRESPOND TO EXPERIMENTAL SEA STATES, WHILE BLACK VALUES CORRESPOND TO EXTRAPOLATED VALUES.

Significant Wave Height (H_s, mm) \ Average Wave Period (T_a, s)	0.67	0.89	1.12	1.34	1.57	1.79	2.01	2.24	2.46	2.68
200	.	.	.	.	1.37	1.37	1.37	1.35	1.34	.
175	.	.	.	1.15	1.16	1.16	1.16	1.14	1.13	.
150	.	.	0.94	0.94	0.95	0.95	**1**	**0.9**	0.92	.
125	.	0.74	0.73	0.73	0.74	0.74	0.73	0.71	0.71	.
100	.	0.53	0.52	0.52	**0.51**	0.53	**0.46**	0.5	0.49	.
75	.	0.32	0.31	0.31	0.32	0.32	0.31	0.29	0.29	.
50	.	0.1	**0.09**	0.11	**0.13**	0.11	**0.11**	0.08	.	.
25	.	0.03	0.02	0.03	0.03	0.03	0.03	0.02	.	.

TABLE V. ELECTRICAL POWER MATRIX FOR THE ACAUSAL CONTROL CASE WITH UNLIMITED REACTIVE POWER FLOW. RED (BOLD) VALUES CORRESPOND TO EXPERIMENTAL SEA STATES, WHILE BLACK VALUES CORRESPOND TO EXTRAPOLATED VALUES.

Significant Wave Height (H_s, mm) \ Average Wave Period (T_a, s)	0.67	0.89	1.12	1.34	1.57	1.79	2.01	2.24	2.46	2.68
200	.	.	.	.	2.15	2.13	2.05	1.96	1.92	.
175	.	.	.	1.82	1.84	1.82	1.73	1.64	1.6	.
150	.	.	1.49	1.5	1.52	1.5	**1.47**	**1.22**	1.28	.
125	.	1.18	1.16	1.18	1.21	1.19	1.1	1	0.96	.
100	.	0.85	0.83	0.85	**0.93**	0.86	**0.83**	0.69	0.64	.
75	.	0.53	0.5	0.52	0.56	0.54	0.46	0.37	0.33	.
50	.	0.21	**0.12**	0.2	**0.23**	0.21	**0.1**	0.06	.	.
25	.	0.05	0.03	0.05	0.06	0.05	0.03	0.02	.	.

TABLE VI. JPD OF NOTIONAL WEC DEPLOYMENT SITE. TABLE VALUES ARE EXPRESSED IN PERCENT. SIGNIFICANT WAVE HEIGHT AND AVERAGE PERIOD HAVE BEEN FROUDE SCALED.

H_s (mm) \ T_a (s)	0.67	0.89	1.12	1.34	1.57	1.79	2.01	2.24	2.46	2.68
200	-	-	-	-	**0.16**	**0.56**	**0.1**	**0.06**	-	-
175	-	-	-	**0.01**	**1.2**	**0.55**	**0.19**	**0.04**	**0.03**	-
150	-	-	-	**0.31**	**2.45**	**0.64**	**0.23**	**0.1**	**0.03**	**0.03**
125	-	-	**0.01**	**2.28**	**2.28**	**1.02**	**0.4**	**0.28**	**0.06**	**0.03**
100	-	-	**0.37**	**6.27**	**3.31**	**1.4**	**0.72**	**0.34**	**0.19**	**0.13**
75	-	**0.02**	**2.78**	**9.88**	**6.5**	**2.84**	**1.09**	**0.92**	**0.46**	**0.09**
50	-	**0.33**	**3.23**	**9.09**	**9.93**	**9.72**	**3.98**	**0.98**	**0.23**	**0.1**
25	**0.01**	**0.14**	**1.04**	**2.03**	**2.6**	**3.35**	**1.4**	**0.2**	**0.06**	**0.01**

The previous results apply for the case of unlimited reactive power flow. It is also important to estimate the electrical power for the case of fully limited reactive power flow as an additional comparison. Since the electrical power has almost no reactive component, the electrical output according to Eq. (9) is essentially the chosen efficiency constant. The power matrix for this limited reactive power case is shown in Table VII. Combining this power matrix with the JPD shown in Table VI indicates a net electrical average annual output of 0.55 W.

This represents 10% increase over the unlimited reactive power case. In terms of annual averaged power production, the case with fully limited reactive power is an 80% improvement over the linear damping case. An intermediate limit on reactive power flow is likely to further increase the output electrical power. The exact amount of reactive power flow will be a function of the efficiency map for a full scale PTO. This will be the subject of future investigations.

V. CONCLUSION

This paper presents results which physically demonstrate the benefit of acausal control strategies using incident wave elevation predictions from an upstream sensor. The results were obtained under irregular wave conditions in real time; necessary requirements for any WEC control scheme.

The results indicate that acausal control can improve the net electrical average annual power by a factor of 1.8 over linear damping control. Further, the algorithm shows a fair degree of robustness when the optimal PTO force profiles are pre-empted by reactive power and force limits.

While the results here were obtained for the case of long crested waves propagating in a single direction, it is hoped that these positive results will provide the impetus to solve the more challenging task of deterministic sea wave prediction for multi-directional seas.

TABLE VII. ELECTRICAL POWER MATRIX FOR THE ACAUSAL CONTROL CASE WITH LIMITED REACTIVE POWER FLOW. RED (BOLD) VALUES CORRESPOND TO EXPERIMENTAL SEA STATES, WHILE BLACK VALUES CORRESPOND EXTRAPOLATED VALUES.

Significant Wave Height (mm) \ Average Wave Period (s)	0.67	0.89	1.12	1.34	1.57	1.79	2.01	2.24	2.46	2.68
200	.	.	.	.	2.39	2.35	2.26	2.15	2.1	.
175	.	.	.	2.02	2.04	2.01	1.91	1.79	1.74	.
150	.	.	1.65	1.67	1.7	1.67	**1.61**	**1.32**	1.38	.
125	.	1.31	1.28	1.31	1.34	1.32	1.21	1.09	1.03	.
100	.	0.95	0.92	0.95	**1.05**	0.96	**0.94**	0.74	0.69	.
75	.	0.59	0.56	0.59	0.62	0.6	0.51	0.4	0.35	.
50	.	0.23	**0.13**	0.22	**0.25**	0.24	**0.1**	0.05	.	.
25	.	0.06	0.03	0.06	0.06	0.06	0.03	0.01	.	.

REFERENCES

[1] J. Hals, J. Falnes, and T. Moan, "A Comparison of Strategies for Adaptive Control of Wave Energy Converters," Journal of Offshore Mechanics and Arctic Engineering, vol.133, pp. 1101-1112, February 2011.

[2] J. Falnes, Ocean Waves and Oscillating Systems: Linear Interaction Including Wave Energy Extraction. Cambridge, UK: Cambridge University Press, 2002.

[3] F. Fusco, and J. Ringwood, "A Study on Prediction Requirements in Real-Time Control of Wave Energy Converters," IEEE Transactions on Sustainable Energy, vol. 3, no. 1, pp. 176-184, January 2012.

[4] M. Belmont, E. Morris, J. Horwood and R. Thurley, "Deterministic Wave Prediction Linked to Wave Energy Absorbers," 3rd European Conf., Patras, Greece, Sept. 1998.

[5] E. Blondel, F. Bonnefoy, and P. Ferrant, "Deterministic non-linear wave prediction using probe data," Ocean Engineering 37, pp. 913-926, 2010.

[6] J. Hals, J. Falnes, and T. Moan, "Constrained Optimal Control of a Heaving Buoy Wave-Energy Converter," Journal of Offshore Mechanics and Arctic Engineering, vol. 133, Feb. 2011.

[7] T. Brekken, "On Model Predictive Control for a Point Absorber Wave Energy Converter," PowerTech, 2011 IEEE Trondheim, pp. 1-8, June 2011.

[8] E. Tedeschi, and M. Molinas, "Tunable Control Strategy for Wave Energy Converters with Limited Power Take-Off Rating,"

IEEE Transactions on Industrial Electronics, vol.51, issue: 10, pp. 3838–3846, Oct 2012.

[9] F. Bretherton, R. Davis, C. Fandry, “A Technique for Objective Analysis and Design of Oceanographic Experiments applied to MODE-73,” Deep Sea Res., 23,pp559-582, 1976.